LVRT Performance of Brushless Doubly Fed Induction Machines - A Comparison

Udai Shipurkar, Tim D. Strous, Henk Polinder, and Jan A. Ferreira

***Abstract*—The Brushless Doubly Fed Induction Machine (B-DFIM) shows promise for use in wind turbine drivetrains. This paper discusses the performance of this machine under symmetric low voltage dips and compares this with the performance of two other machines - the Permanent Magnet Synchronous Machine (PMSM) and the Doubly-Fed Induction Generator (DFIG). Attention is paid to the controller for the B-DFIM and protection methods for improved Low Voltage Ride Through (LVRT) performance are discussed. It is shown that the B-DFIM has an improved LVRT performance when compared with the DFIG, moreover, the B-DFIM does not require an external circuit for protection from low voltage events.**

***Index Terms*—Brushless Doubly-Fed Machine (BDFM), DFIG, PMSM, LVRT.**

I. Introduction

With growing interest in sustainable forms of energy, the wind industry is growing rapidly. The DFIG is a popular choice for the wind turbine drivetrain because it is cost effective. However, it suffers from reliability and maintenance issues due to the slip rings and brushes it requires. The B-DFIM aims at addressing these drawbacks.

With increased wind power penetration, it is no longer acceptable for wind turbines to trip during grid disturbances. Therefore, the study of the performance of wind turbine drivetains under low voltage events is important. However, there has been little research on the LVRT performance of the B-DFIM. Shao *et al.* studied the dynamic behaviour of the machine during symmetrical voltage dips [1]. This study was limited as it did not consider the subsequent voltage rise of the grid and it did not propose any methods to improve the performance. In 2011 they proposed a control scheme that gives the B-DFIM the capability to ride through low voltage faults [2] and this was extended for asymmetric low voltage faults [3].

This paper develops a controller for the B-DFIM as part of a wind turbine drivetrain. This controller is based on vector control and consists of cascaded current control loops - one for the power winding current and the inner loop for the control winding current. The paper looks at the generation of the reference signal (P_p^{ref}) which is required for the control. The paper also investigates the performance of the B-DFIM under symmetric low voltage events and compares this with the performance of PMSM and DFIG based drivetrains. This comparison is done on machines that have been designed for the same wind turbine drivetrain and have similar design parameters such as air-gap length, air gap radius and rated speeds. This similarity provides a good foundation for a comparison in performance.

Section II describes the dynamic model of the B-DFIM. Section III develops the vector control for the machine and describes the method of generating the reference signals. Section IV investigates the performance of the PMSM, DFIG and B-DFIM machines under conditions of a low voltage event on the grid. It also describes methods of improving the LVRT response of these machines. Finally Section V draws some conclusions from the study.

The research leading to these results has received funding from the European Union's Seventh Framework Programme managed by REA Research Executive Agency (FP7/2007_2013) under Grant Agreement N.315485.

U. Shipurkar, T. D. Strous, H. Polinder and J. A. Ferreira are with the Department of Electrical Sustainable Energy, Delft University of Technology, The Netherlands (e-mail: u.shipurkar@tudelft.nl)

II. B-DFIM Dynamic Model

The equations representing the B-DFIM dynamic model are derived from the equivalent circuit of the B-DFIM which has been extensively covered in literature [4]–[9]. These are reproduced below in an arbitrary reference frame *'k'* rotating with a speed of ω_k with respect to the power winding stator reference frame.

$$\bar{u}_p^k = R_p \bar{i}_p^k + \omega_k \begin{bmatrix} 0 & -1 \\ 1 & 0 \end{bmatrix} \bar{\lambda}_p^k + \frac{d\bar{\lambda}_p^k}{dt} \tag{1}$$

$$\bar{u}_c^k = R_c \bar{i}_c^k + (\omega_k - (p_p + p_c)\omega_m) \begin{bmatrix} 0 & -1 \\ 1 & 0 \end{bmatrix} \bar{\lambda}_c^k + \frac{d\bar{\lambda}_c^k}{dt} \tag{2}$$

$$0 = R_r \bar{i}_r^k + (\omega_k - p_p\omega_m) \begin{bmatrix} 0 & -1 \\ 1 & 0 \end{bmatrix} \bar{\lambda}_p^k + \frac{d\bar{\lambda}_r^k}{dt} \tag{3}$$

and,

$$\begin{bmatrix} \bar{\lambda}_p^k \\ \bar{\lambda}_c^k \\ \bar{\lambda}_r^k \end{bmatrix} = \left(\begin{bmatrix} L_p & 0 & M_{pr} \\ 0 & L_c & -M_{cr} \\ M_{pr} & -M_{cr} & L_r \end{bmatrix} \right) \begin{bmatrix} \bar{i}_p^k \\ \bar{i}_c^k \\ \bar{i}_r^k \end{bmatrix} \tag{4}$$

To complete the dynamic model, the equation of torque is derived from the expression of power. (5) gives the expression for electric power at the terminal of a stator winding.

$$p_s = \bar{u}_{s,abc}^T \bar{i}_{s,abc} \tag{5}$$

using Clark's transformation, this expression is expressed in the stationary reference frame as seen in (6).

$$p_s = \bar{i}_s^{sT} \bar{u}_s^s \tag{6}$$

Using the voltage equations in the stationary reference frame,

the expression for power is expressed as,

$$p_s = R_s \bar{i}_s^{sT} \bar{i}_s^s + (L_{s,\sigma} + L_{s,m}) \bar{i}_s^{sT} \begin{bmatrix} 0 & -1 \\ 1 & 0 \end{bmatrix} \bar{i}_s^s p \frac{d\theta}{dt} + M_{sr} \bar{i}_s^{sT} \begin{bmatrix} 0 & -1 \\ 1 & 0 \end{bmatrix} \bar{i}_r^s p \frac{d\theta}{dt} \quad (7)$$

It can be seen that the first term represents the resistance loss in the winding, the second term will be equal to zero and the remaining term represents the power converted into mechanical power. The torque is given by,

$$p_m = T_e \frac{d\theta}{dt} \quad (8)$$

Therefore, the electromagnetic torque can be expressed as,

$$T_e = p M_{sr} \bar{i}_s^{sT} \begin{bmatrix} 0 & -1 \\ 1 & 0 \end{bmatrix} \bar{i}_r^s \quad (9)$$

This expression is extended to form the torque expression for the B-DFIM by including both the stator windings. If the Park's transform is used, the equation in the stationary reference frame may be converted to a rotating reference frame,

$$T_e = p_p M_{pr} (i_p^{k,q} i_r^{k,d} - i_p^{k,d} i_r^{k,q}) + p_c M_{cr} (i_c^{k,q} i_r^{k,d} - i_c^{k,d} i_r^{k,q}) \quad (10)$$

III. B-DFIM Control

This section describes the vector control scheme used in the control of the B-DFIM. This scheme is along the lines investigated in [10]–[12]. Here, a method of generating the reference power signal is also described.

A. Active Power Control

A reference frame rotating with the Power Winding flux is chosen and results in (11) and (12) for the d and q components of Power Winding flux.

$$\lambda_p^{PW,d} = |\lambda_p| \quad (11)$$

$$\lambda_p^{PW,q} = 0 \quad (12)$$

This reference frame is referred to as the PW reference frame in the rest of this document. If the assumption is made that U_p is constant and R_p is small enough to be neglected, the flux $|\lambda_p|$ will be constant. This gives,

$$R_p (i_p^{PW,d} i_p^{PW,d} + i_p^{PW,q} i_p^{PW,q}) \approx 0 \quad (13)$$

$$\frac{d|\lambda_p|}{dt} \approx 0 \quad (14)$$

Therefore, P_p simplifies to,

$$P_p \approx \omega_k |\lambda_p| i_p^{PW,q} \quad (15)$$

Therefore, a reference power winding current signal can be generated from a reference P_p signal using (16).

$$i_p^{PW,q-ref} = \frac{P_p^{ref}}{\omega_k |\lambda_p|} \quad (16)$$

For this machine, only the control winding circuit is controllable through the power electronic converter. Therefore, the next step would be to obtain a reference $i_c^{PW,q}$ current. Consider the flux equations,

$$\bar{\lambda_p}^{PW} = L_p \bar{i_p}^{PW} + M_{pr} \bar{i_r}^{PW} \quad (17)$$

$$\bar{\lambda_c}^{PW} = L_c \bar{i_c}^{PW} - M_{cr} \bar{i_r}^{PW} \quad (18)$$

$$\bar{\lambda_r}^{PW} = L_r \bar{i_r}^{PW} + M_{pr} \bar{i_p}^{PW} - M_{cr} \bar{i_c}^{PW} \quad (19)$$

From these equations the relation between the power winding and control winding currents is given by,

$$i_c^{PW,d} = \frac{1}{L_c} \lambda_c^{PW,d} - \frac{M_{cr} L_p}{M_{pr} L_c} i_p^{PW,d} + \frac{M_{cr}}{M_{pr} L_c} |\lambda_p| \quad (20)$$

$$i_c^{PW,q} = \frac{1}{L_c} \lambda_c^{PW,q} - \frac{M_{cr} L_p}{M_{pr} L_c} i_p^{PW,q} \quad (21)$$

From (21) it is seen that $i_c^{PW,q}$ depends on $i_p^{PW,q}$ and $\lambda_c^{PW,q}$. $\lambda_c^{PW,q}$ is weakly dependant on $i_p^{PW,d}$ and $i_c^{PW,d}$. This influence of $d-$axis terms on $q-$axis quantities and vice versa is termed 'Cross-Coupling'. For accurate control it is required that the d and q axis terms be completely de-coupled such that the control of both parameters is independent of the other. However, in the simulations here, the effect of this cross-coupling has been found to be small and is neglected. Further, it is also seen that $i_c^{PW,q}$ varies with $-i_p^{PW,q}$.

The power electronic converter can be controlled by the duty ratio for the switches, which can be calculated from the reference control winding voltage and the DC bus voltage. For the simulations here, the reference voltage u_c is used as input to the machine. The dependence of u_c^q on i_c^q can be calculated from the control winding voltage equation in (22).

$$u_c^{PW,q} = R_c i_c^{PW,q} + (\omega_{PW} - (p_p + p_c)\omega_m) \lambda_c^{PW,d} + \frac{d\lambda_c^{PW,q}}{dt} \quad (22)$$

A similar cross-coupling term, due to $\lambda_c^{PW,d}$ is seen in the equation above. This can also be expressed as in (23). This has been taken into account in the controller.

$$u_c^{PW,q} = f(i_c^{PW,q}, \lambda_c^{PW,q}) + \underbrace{(\omega_{PW} - (p_p + p_c)\omega_m)(\frac{L_p M_{cr}}{M_{pr}} i_p^{PW,d} + L_c i_c^{PW,d})}_{\text{Cross-Coupling Term}} \quad (23)$$

The complete control scheme for Active Power control of the B-DFIM is shown in Fig. 1.

B. Reactive Power Control

The Reactive Power of the Power Winding for the B-DFIG in the arbitrary reference frame 'k' is given by,

$$Q_p = u_p^{k,q} i_p^{k,d} - u_p^{k,d} i_p^{k,q} \quad (24)$$

Substituting the voltage equation in (24) gives,

$$Q_p = i_p^{k,d} \frac{d\lambda_p^{k,q}}{dt} + \omega_k i_p^{k,d} \lambda_p^{k,d} - i_p^{k,q} \frac{d\lambda_p^{k,d}}{dt} + \omega_k i_p^{k,q} \lambda_p^{k,q} \quad (25)$$

Again, the PW reference frame is chosen ((11) and (12)) and U_p is assumed to be constant and R_p is neglected. The expression for Q_p can be expressed as,

$$Q_p \approx \omega_{PW}|\lambda_p^d| i_p^{PW,d} \tag{26}$$

The reference power winding current signal can be generated from the reference Q_p signal using (27).

$$i_p^{PW,d-ref} = \frac{Q_p^{ref}}{\omega_{PW}|\lambda_p|} \tag{27}$$

From (20) it is seen that $i_c^{PW,d}$ depends on $i_p^{PW,d}$ and $\lambda_c^{PW,d}$. $\lambda_c^{PW,d}$ is weakly dependant on $i_p^{PW,q}$ and $i_c^{PW,q}$. Again there is a dq cross-coupling term which must be compensated for.

The dependence of $u_c^{PW,d}$ on $i_c^{PW,d}$ can be calculated from the Control Winding voltage equation.

$$\begin{aligned} u_c^{PW,d} &= R_c i_c^{PW,d} - (\omega_{PW} - (p_p + p_c)\omega_m)\lambda_c^{PW,q} \\ &\quad + \frac{d\lambda_c^{PW,d}}{dt} \end{aligned} \tag{28}$$

Again, we see a dq cross-coupling term due to $\lambda_c^{PW,q}$. This can be seen in (29).

$$\begin{aligned} u_c^{PW,d} &= f(i_c^{PW,d}, \lambda_c^{PW,d}) \\ &\quad \underbrace{- (\omega_{PW} - (p_p + p_c)\omega_m)(\frac{L_p M_{cr}}{M_{pr}} i_{PW,p}^q + L_c i_c^{PW,q})}_{\text{Cross-Coupling Term}} \end{aligned} \tag{29}$$

The complete Reactive Power control scheme is shown in Fig. 1.

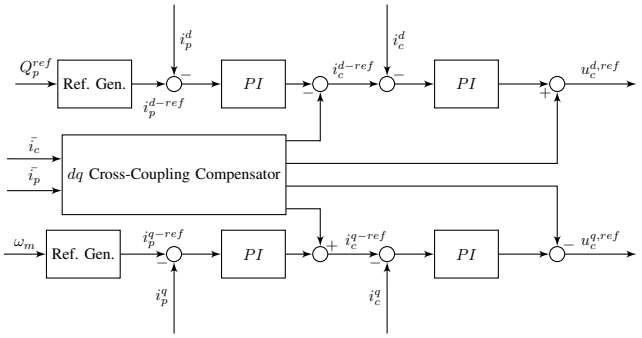

Fig. 1. B-DFIG Control Scheme

C. Reference Signal Generation

When such a machine is used in a wind turbine drivetrain, the reference power signal is chosen so as to extract the maximum energy from the blades. Therefore, this section describes the generation of such a P_p^{ref} signal from the rotational angular velocity of the machine rotor.

The aim of the control scheme is to maximise the power output of the wind turbine. A typical wind turbine characteristics with the optimal power extraction-speed curve and its intersection with the $C_{p,max}$ for all wind speeds [13] is shown in Fig. 2. As P_{opt} is the curve with $C_{p,max}$ it is evident that if the turbine is controlled and kept on this curve, the turbine will generate the maximum energy. This is followed for all speeds below rated. For speeds above rated, rated power P_{rated} is maintained. This is described in (30).

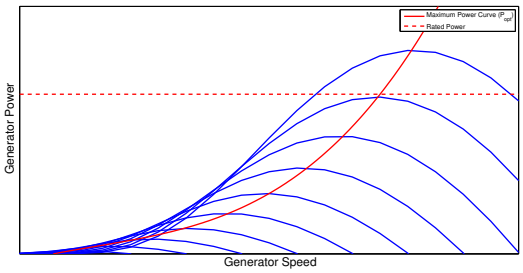

Fig. 2. Control Strategy for Optimal Power Extraction. The plot shows the generator output power vs. speed curve for different wind speeds. The P_{opt} curve connects all the points of maximum power forming the curve for optimal power extraction.

$$P_{ref} = \begin{cases} \frac{1}{2}\frac{\rho A R^3 C_{p,max}}{\lambda_{t,max}^3}\omega_m^3 & \text{if } \omega_m < \omega_{rated} \\ P_{rated} & \text{if } \omega_m \geq \omega_{rated} \end{cases} \tag{30}$$

where $\lambda_{t,max}$ is the tip speed ratio for $C_{p,max}$. Section III-A discusses the control of the machine, this control is based on the Active Power of the Power Winding alone. Therefore, it is required to generate the control signal (P_p^{ref}) from the rotor speed (ω_m).

The steady state characteristics are used to generate a function for the relation between ω_m and P_p^{ref}. The characteristics depend on two variables, i.e. magnitude of the Control Winding voltage and the phase angle between Control Winding and Power Winding voltages. Therefore, given a value of ω_m and P^{ref} there are a number of operating points possible. To select an optimal operating point the efficiency of the machine is used as a selection criteria. Solving the system for maximum efficiency, the curve for the Power Winding Power corresponding to each point of the net power curve is shown in Fig. 3. The figure follows the motor convention and the power is (-)ve when the machine is generating power.

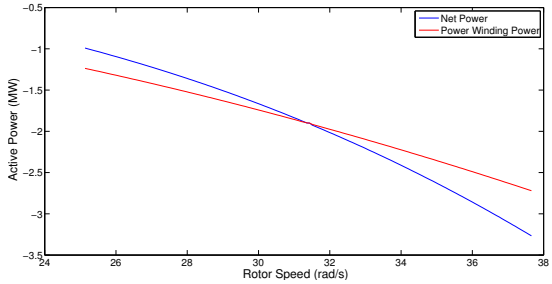

Fig. 3. Curve for net Shaft Power and Power Winding Active Power based on maximising Efficiency.

IV. LVRT Performance

The symmetric voltage dip considered here is shown in Fig. 4. The details of the machines used and the parameters on which the design of the machines is based are given in the Appendix. At the instant of the low voltage event, the machines are delivering rated power and the wind speed is assumed to be constant through the event.

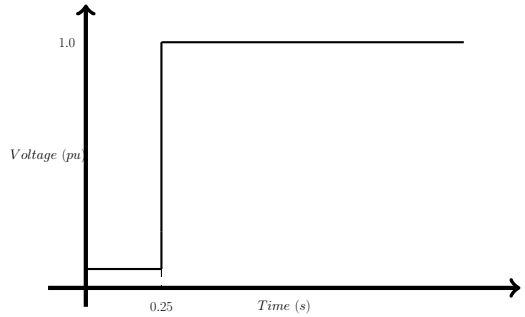

Fig. 4. Voltage Profile for LVRT Response Study

A. PMSM Performance

The PMSM is completely isolated from the grid through an AC-DC-AC converter. Therefore, disturbances on the grid do not directly affect the machine. However, in the occurrence of an LVRT event, the ability of the grid side converter to transfer power to the grid is greatly reduced. This results in the rise in voltage of the DC link which is a cause for concern for the DC link capacitors.

Fig. 5 shows the response of the machine when it encounters a 95% symmetric voltage dip as shown in Fig. 4.

Fig. 5a and Fig. 5b show that there is little effect of the low voltage event on the machine. However, Fig. 5d shows that the DC voltage rise is indeed an issue.

A number of methods have been devised to address this issue. One such method is the use of Energy Discharge Circuits [14]. This limits the rise of the DC link voltage by using resistive elements to dissipate a part of the power fed to the DC circuit through the generator side converter. The DC-link voltage with such a technique is shown in Fig. 5d. Another method used is the use of Energy Storage Systems [14] to manage and store the excess energy during low voltage events. Other methods include Power Balancing [15] where the generator side converter is made to follow the grid side converter during low voltage events reducing the electrical torque such that the power output to the DC-link equal the power fed to the grid. Thus, the turbine speeds up and stores the extra energy as rotational energy. This reduces the power mismatch during such events and hence reduces the DC link voltage rise.

B. DFIG Performance

Unlike the PMSM, the DFIG is not isolated from the grid. The stator of the machine is connected directly to the grid and any disturbance in the form of a low voltage event can be

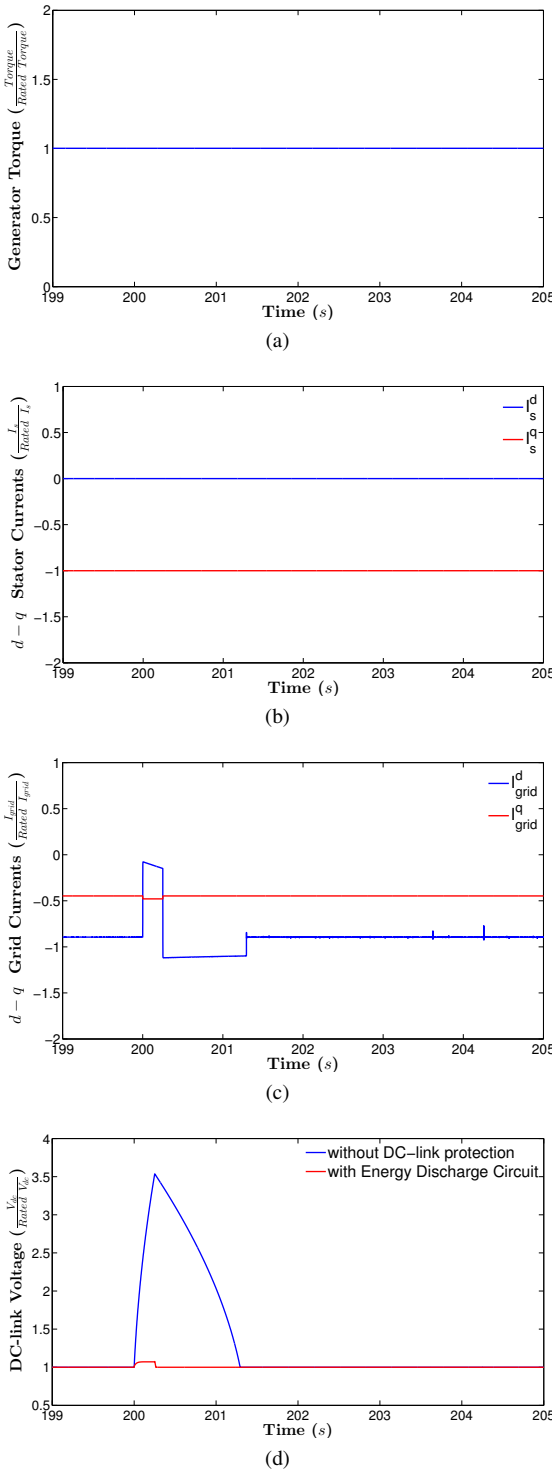

Fig. 5. LVRT Performance of PMSM for a 95% Symmetric Voltage Dip at t=200s (a) Generator Torque (b) Stator Currents in the Stator Flux reference frame (c) Grid Currents in the Grid Reference Frame (d) DC link voltage

expected to have an effect on the stator and rotor currents. During the Low Voltage event, large transient currents are induced in the stator winding. Such transient currents are also induced in the rotor circuit due to the magnetic coupling of the stator and rotor circuits. This is dangerous to the power

electronic converter connected to the rotor circuit.

A widely used method for the protection of the DFIG under low voltage events is the Crowbar circuit [14]. The crowbar circuit is a set of switches and resistors that short circuit the rotor terminals through the resistors in the case of the low voltage event and by-pass the generator side converter. The response of the DFIG with a Crowbar circuit during a Low Voltage event is shown in Fig. 6. The connection of the crowbar circuit serves a number of purposes. First, it bypasses the power electronic converter when large transient rotor currents are present. This protects the converter in the event of a Low Voltage event. Second, the added resistance in the rotor circuit lowers the magnitude of the transient rotor currents. Third, the added resistance in the crowbar circuit reduces the time constant of the rotor circuit ($\tau_r = \frac{L_r}{R_r+R_{crowbar}}$), this means that the currents during the fault will decay faster.

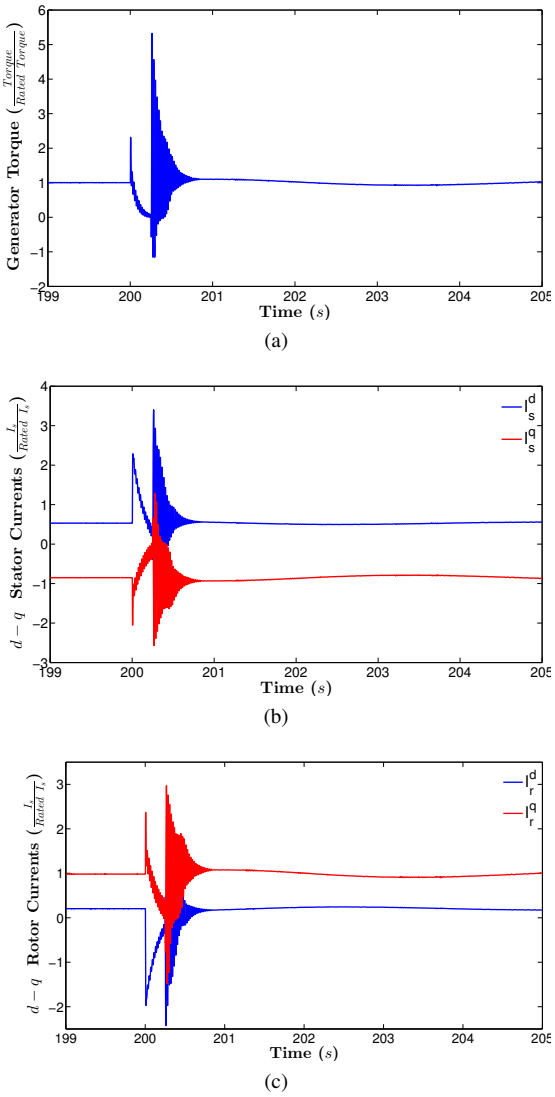

Fig. 6. LVRT Performance of DFIG for a 95% Symmetric Voltage Dip at t=200s (a) Generator Torque (b) Stator Currents in the Stator Flux reference frame (c) Rotor Currents in the Stator Flux reference frame

There are however a number of issues with the use of the crowbar circuit as well. First, when the crowbar circuit is activated, the DFIG resembles a induction motor with an external rotor resistance. This would mean that the machine would absorb reactive power from the grid which may further exasperate the condition of the grid. Second, the vector control is lost during the action of the crowbar circuit and re-establishing control after the crowbar is released could be a challenge.

C. B-DFIM Performance

The B-DFIM suffers from the same issues faced by the DFIG under low voltage events. However, the magnitude of the transient currents in the control circuit is lower in the B-DFIM than that in the DFIG. This can be attributed to the larger leakage inductance of the B-DFIM.

Although the B-DFIM could also be protected against the effects of a low voltage event by the use of a Crowbar circuit, this machine can be protected without the use of an external circuit and with the use of an addition in the control algorithm. This is shown in Fig. 7.

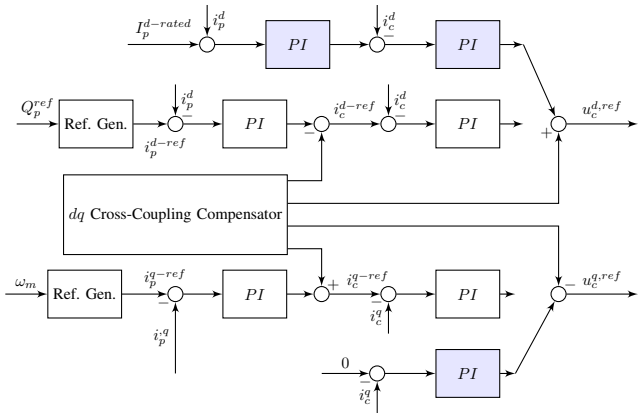

Fig. 7. B-DFIM Control Scheme with LVRT Protection. The figure shows the added control loops that are used during the low voltage event

Crowbarless protection is achieved by detecting a low voltage event and setting the reference value of the inner control winding current loop q-reference to zero. Also, the d-reference I_p value is set to the rated current in order to injective reactive current for grid support.

Fig. 8 shows the performance of the B-DFIM with the Crowbarless protection which has also been discussed in [16].

Section III-A and Section III-B has discussed the calculation of the i_p^{d-ref} and i_p^{q-ref} reference signal depends on the d-axis power winding flux. Therefore, in the case of a low voltage event it is required to maintain pre-fault reference values.

Here, the focus has been on the control winding currents in the B-DFIM as they affect the power electronic converter directly. It has been seen that the transients in the power winding currents are high and need to be investigated further. However, the control winding currents are reduced, this is attributed to higher leakage inductances in the B-DFIM. The torque oscillations are also lower in the B-DFIM especially at the instant of of grid recovery. This paper has not dealt with

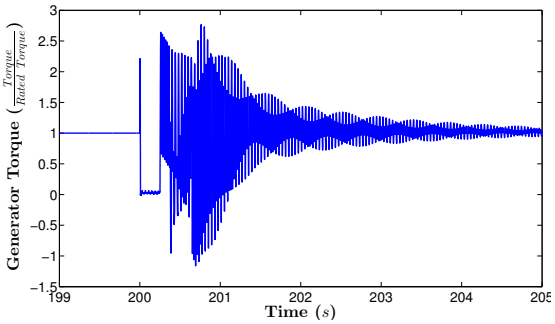

(a)

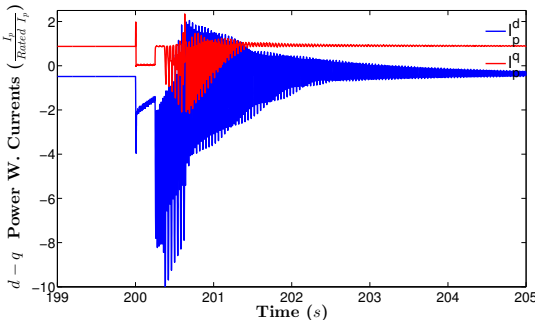

(b)

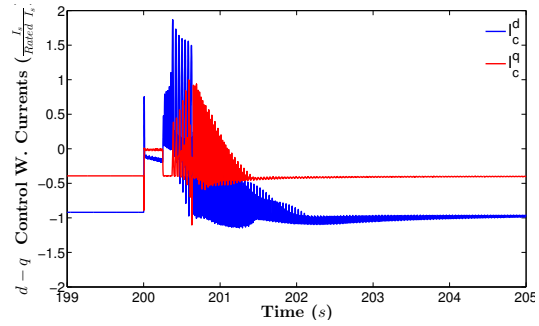

(c)

Fig. 8. LVRT Performance of B-DFIM with Crowbarless Protection for a 95% Symmetric Voltage Dip (a) Generator Torque (b) Power Winding Currents in the PW Reference Frame (c) Control Winding Currents in the PW Reference Frame

reactive current injection of the B-DFIM in detail and that should be investigated further.

V. Conclusion

For the PMSM based wind turbine, the issue with Low Voltage Ride Through (LVRT) is the rise in the DC link voltage . This is due to the mismatch in power generated by the machine and the power transferred to the grid.

For the DFIG it has been found that voltage dips cause large transient currents in the stator and rotor circuit. The oscillations in the rotor circuit are cause for concern as they may lead to adverse effects on the power electronic converter connected to the circuit. A possible method to overcome this issue is the use of a Crowbar circuit. The crowbar circuit manages the problem by bypassing the power electronic converter in the event of current rise. Additionally, the crowbar resistors reduce the time constant of the rotor circuit, allowing for a faster decay of transient currents.

In the case of the B-DFIM, it has been found that again transient currents are set up in the power and control windings in the event of a voltage dip. However, the magnitude of these currents in the control winding is lower when compared to that of the rotor currents in the DFIG. This is attributed to the higher leakage inductance of the B-DFIG. A Crowbarless method has also been discussed which is successful in controlling the high currents generated in the control winding. This Crowbarless control method also reduces the torque oscillations observed in the B-DFIM for a low voltage event.

Fig. 9 compares the magnitude of torque and rotor and control winding currents in the BDFIM and DFIG.

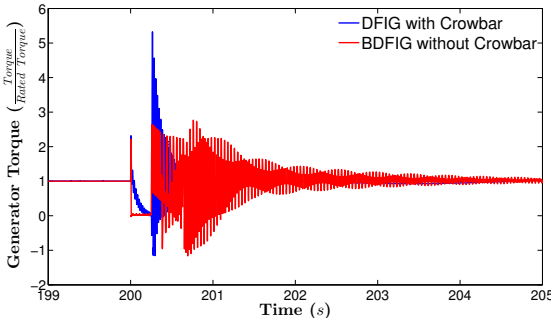

(a)

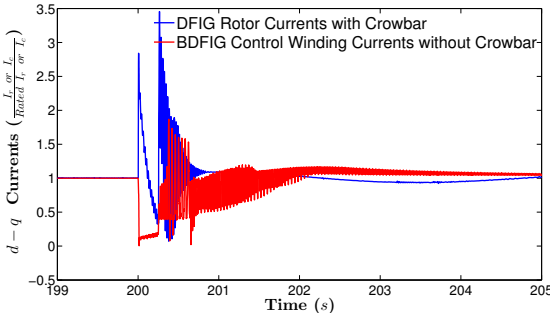

(b)

Fig. 9. Comparison between BDFIM and DFIG performance a) Torque and b) Rotor and Control Winding Currents

In conclusion, apart from offering better reliability through the exclusion of slip ring and brushes, the B-DFIG also has an improved LVRT performance when compared with the DFIG. The protection does not require an external circuit, like the crowbar, and can be built into the machine controller.

Appendix

The parameters on which the design of the three machines is based are given in Table I, The equivalent circuits of the three machines used in the simulations are given below,

TABLE I
DESIGN PARAMETERS

		PMSM	DFIG	B-DFIM
Number of Pole Pairs		11	13	4&6
Gearbox Ratio		23	23	30
Rated Electrical Frequency	Hz	51.02	50.30	50&20
Rated Generator Speed	rpm	278.3	278.3	275
Stator Outer Radius	m	0.85	0.86	0.83
Stack Length	m	0.63	0.97	1.57
Rotor Inner Radius	m	0.66	0.66	0.58
Air-Gap Length	mm	2.58	2.58	2.58
Ratio Length-Diameter		0.37	0.57	0.95
Ratio Slot Height-Width		1.91	1.15	2.35
Stator Yoke Width	mm	52.07	46.52	80
Stator Slot Width	mm	34.71	31.01	29.7

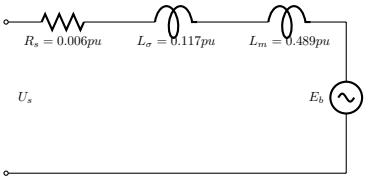

Fig. 10. PMSM Equivalent Circuit

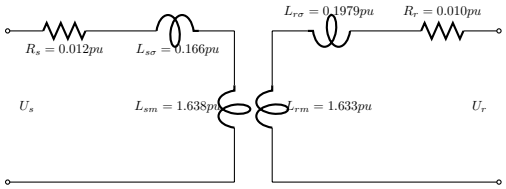

Fig. 11. DFIG Equivalent Circuit

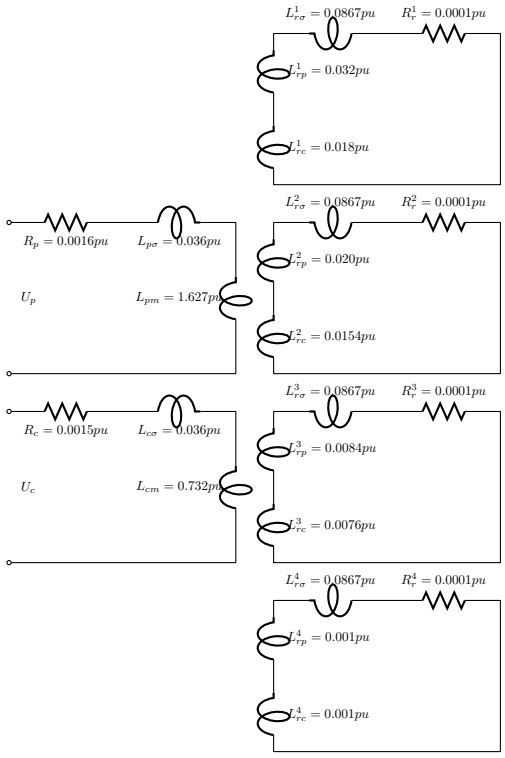

Fig. 12. B-DFIM Equivalent Circuit

REFERENCES

[1] S. Shao, E. Abdi, and R. McMahon, "Dynamic Analysis of the Brushless Doubly-Fed Induction Generator during Symmetrical Three-Phase Voltage Dips," *International Conference on Power Electronics and Drive Systems*, pp. 464–469, 2009.

[2] S. Shao, T. Long, E. Abdi, R. McMahon, and Y. Wu, "Symmetrical Low Voltage Ride-Through of the Brushless Doubly-Fed Induction Generator," *IEEE Industrial Electronics Society Conference*, pp. 3209–3214, 2011.

[3] T. Long, S. Shao, E. Abdi, R. a. McMahon, and S. Liu, "Asymmetrical Low-Voltage Ride Through of Brushless Doubly Fed Induction Generators for the Wind Power Generation," *IEEE Transactions on Energy Conversion*, vol. 28, no. 3, pp. 502–511, Sep. 2013. [Online]. Available: http://ieeexplore.ieee.org/lpdocs/epic03/wrapper.htm?arnumber=6544266

[4] R. Li, A. Wallace, and R. Spée, "Dynamic Simulation of Brushless Doubly-Fed Machines," *IEEE Transactions on Energy Conversion*, vol. 6, no. 3, pp. 445–452, 1991.

[5] R. Li, R. Spee, A. Wallace, and G. Alexander, "Synchronous drive performance of brushless doubly-fed motors," *IEEE Transactions on Industry Applications*, vol. 30, no. 4, pp. 963–970, 1994.

[6] M. S. Boger, A. K. Wallace, R. Spée, and R. Li, "General Pole Number Model of the Brushless Doubly-Fed Machine," *IEEE Transactions on Industry Applications*, vol. 31, no. 5, pp. 1022–1028, 1995.

[7] B. Gorti, G. Alexander, and R. Spee, "Power Balance Considerations for Brushless Doubly-Fed Machines," *IEEE Transactions on Energy Conversion*, vol. 11, no. 4, pp. 687–692, 1996.

[8] R. A. McMahon, P. C. Roberts, X. Wang, and P. J. Tavner, "Performance of BDFM as generator and motor," *IEE Proceedings - Electric Power Applications*, vol. 153, no. 2, pp. 289–299, 2006.

[9] R. a. McMahon, X. Wan, E. Abdi-Jalebi, P. J. Tavner, P. C. Roberts, and M. Jagiela, "The BDFM as a Generator in Wind Turbines," *2006 12th International Power Electronics and Motion Control Conference*, pp. 1859–1865, Aug. 2006. [Online]. Available: http://ieeexplore.ieee.org/lpdocs/epic03/wrapper.htm?arnumber=4778676

[10] F. Barati, R. McMahon, S. Shao, E. Abdi, and H. Oraee, "Generalized Vector Control for Brushless Doubly Fed Machines With Nested-Loop Rotor," *IEEE Transactions on Industrial Electronics*, vol. 60, no. 6, pp. 2477–2485, Jun. 2013. [Online]. Available: http://ieeexplore.ieee.org/lpdocs/epic03/wrapper.htm?arnumber=6339050

[11] E. Abdi, F. Barati, and R. McMahon, "Stator-Flux-Oriented Vector Control for Brushless Doubly Fed Induction Generator," *IEEE Transactions on Industrial Electronics*, vol. 56, no. 10, pp. 4220–4228, Oct. 2009. [Online]. Available: http://ieeexplore.ieee.org/lpdocs/epic03/wrapper.htm?arnumber=5071226

[12] J. Poza, E. Oyarbide, I. Sarasola, and M. Rodriguez, "Vector control design and experimental evaluation for the brushless doubly fed machine," *IET Electric Power Applications*, vol. 3, no. 4, pp. 247–256, 2009. [Online]. Available: http://digital-library.theiet.org/content/journals/10.1049/iet-epa.2008.0090

[13] R. Pena, J. Dlare, and G. Asher, "Doubly fed induction generator uising back-to-back PWM converters and its application to variable- speed wind-energy generation," *IEE Proc.-Electr. Power Appl.*, vol. 143, no. 3, pp. 231–241, 1996.

[14] C. Abbey, W. Li, L. Owatta, and G. Joos, "Power Electronic Converter Control Techniques for Improved Low Voltage Ride Through Performance in WTGs," *Power Electronics Specialists Conference*, pp. 1–6, 2006.

[15] X.-P. Yang, X.-F. Duan, F. Feng, and L.-L. Tian, "Low Voltage Ride-Through of Directly Driven Wind Turbine with Permanent Magnet Synchronous Generator," *2009 Asia-Pacific Power and Energy Engineering Conference*, pp. 1–5, Mar. 2009. [Online]. Available: http://ieeexplore.ieee.org/lpdocs/epic03/wrapper.htm?arnumber=4918470

[16] T. Long, S. Shao, P. Malliband, E. Abdi, and R. McMahon, "Crowbarless Fault Ride-Through of the Brushless Doubly Fed Induction Generator in a Wind Turbine Under Symmetrical Voltage Dips," *IEEE Transactions on Industrial Electronics*, vol. 60, no. 7, pp. 2833–2841, 2013.